CHEMICAL PHYSICS

Crossover from hydrogen to chemical bonding

Bogdan Dereka[1], Qi Yu[2]*, Nicholas H. C. Lewis[1], William B. Carpenter[1], Joel M. Bowman[2], Andrei Tokmakoff[1]†

Hydrogen bonds (H-bonds) can be interpreted as a classical electrostatic interaction or as a covalent chemical bond if the interaction is strong enough. As a result, short strong H-bonds exist at an intersection between qualitatively different bonding descriptions, with few experimental methods to understand this dichotomy. The $[F\text{-}H\text{-}F]^-$ ion represents a bare short H-bond, whose distinctive vibrational potential in water is revealed with femtosecond two-dimensional infrared spectroscopy. It shows the superharmonic behavior of the proton motion, which is strongly coupled to the donor-acceptor stretching and disappears on H-bond bending. In combination with high-level quantum-chemical calculations, we demonstrate a distinct crossover in spectroscopic properties from conventional to short strong H-bonds, which identify where hydrogen bonding ends and chemical bonding begins.

Qualitatively, a hydrogen bond (H-bond) is an attractive interaction between an acceptor (A) and a hydrogen atom covalently bonded to a donor (D), but quantitative descriptions of H-bonds have been debated since their inception (*1*, *2*). Conventional H-bonds are commonly described through the electrostatic attraction between the positive proton charge and the electronegative acceptor, and their presence is revealed in the separation and linearity of the D-H···A atoms and a decrease in D-H vibrational frequency. Questions about the adequacy of these classical concepts arise when considering short strong H-bonds (SHBs). They can have interaction strengths similar to those of covalent bonds, protons appearing shared between D and A, and could involve substantial electronic redistribution across the bonded atoms (*3*, *4*). As a result, it may be better to describe SHBs as covalent three-center four-electron bonds, rather than as a classical electrostatic phenomenon (*5*). Where do hydrogen bonds end and covalent bonds begin? This question has implications in processes involving SHBs—for instance, in biomolecular processes such as enzymatic catalysis (*3*, *4*, *6*–*8*), signaling (*9*), and ligand binding (*10*, *11*), as well as atmospheric and interstellar chemistry (*12*, *13*), proton transport (*9*, *14*, *15*), and ion hydration (*16*–*18*). There is a debate about how large the SHB energies are and if they can survive the strong solvation interactions in water and polar environments (*19*–*21*). Therefore, experiments are needed to characterize the physical and chemical properties of SHBs.

H-bonding phenomena express themselves quantitatively in the shape of the electronic potential energy experienced by the proton along the H-bond. In conventional H-bonds, the donor–acceptor separation is large (>2.7 Å), and the potential minimum is localized near D at its covalent D-H bond length (Fig. 1A) (*3*, *4*, *22*). As the D···A distance shrinks and the H-bond strength increases, the barrier decreases until the zero-point energy of the proton exceeds it and ultimately yields a flat-bottom single-well potential. It corresponds to the SHB regime in which the proton becomes a confined particle delocalized between D and A. The potential energy surface is a key descriptor linking the underlying quantum-mechanical electronic structure of the D-H···A H-bond to experimental observables.

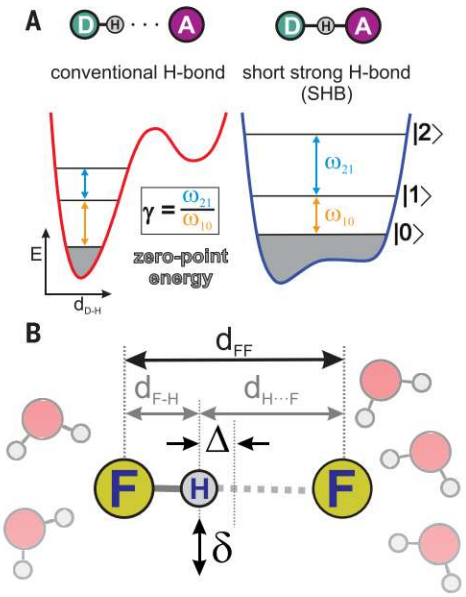

Fig. 1. Hydrogen bonds. (**A**) Types of hydrogen bonds depending on donor-acceptor distance. Potentials of proton motion are shown along with the first three quantum levels and the associated lowest-energy transitions. (**B**) Principal coordinates of any H-bond demonstrated with $HF_2^-{}_{(aq)}$: donor-acceptor distance (d_{FF}), proton asymmetry (Δ), and linearity (δ).

Despite being the most common H-bond metric, the D···A distance cannot be easily related to the shape of the hydrogen bond potential, but infrared (IR) vibrational spectroscopy can directly characterize it. The D-H vibrational frequency decreases with increasing H-bond strength, a textbook property of an H-bond; however, the fundamental frequency itself is not a descriptor of the proton potential. The vibrations of protons in H-bonds deviate greatly from harmonic oscillations, and their anharmonicity and mode mixing with the D···A stretching and H-bond bending vibrations are major factors influencing the structure, dynamics, and reactivity of H-bonds. A more useful measurement is to observe how the vibrational transition frequencies depend on quantum numbers 0, 1, and 2 (Fig. 1A). Conventional H-bonds follow traditional rules for anharmonic vibrations, in which the vibrational energy splitting decreases as one ascends the vibrational ladder (positive anharmonicity). The $|0\rangle$ to $|1\rangle$ transition frequency ω_{10} is larger than the $|1\rangle$ to $|2\rangle$ frequency ω_{21}, as characterized by their ratio $\gamma = \omega_{21}/\omega_{10} < 1$. By contrast, when proton confinement dictates the potential shape in SHBs, the spacing between states increases up the vibrational ladder (analogous to a particle-in-a-box) and $\gamma > 1$ (negative anharmonicity), yielding the effect called superharmonicity.

Experimental results

We investigated an SHB in aqueous solution by characterizing the anharmonic potential of its multiple coupled vibrations, and we addressed how electronic structure becomes an important consideration in the transition from conventional to strong H-bonds. We used a combination of femtosecond two-dimensional infrared (2D IR) spectroscopy and high-level anharmonic quantum-chemical calculations to directly demonstrate the distinctive nature and characteristics of elusive SHBs in water using the bifluoride anion HF_2^- as a model system. Bifluoride is a linear symmetric ion with the proton bridging two fluorine atoms, which represents the ideal model of a bare H-bond and allows one to study SHBs in room-temperature liquid solution (*23*). The extremely short F-F separation puts it into the category of single-well H-bonds (Fig. 1 and fig. S3) and makes it the strongest H-bond, with an energy of 45.8 kcal/mol (*24*).

The infrared spectrum of aqueous KHF_2 is shown in Fig. 2A with the assignment of vibrational modes that report on the principal geometric coordinates of any H-bond (Fig. 1B). On the basis of gas-phase, solid-state, and theoretical studies (*23*, *25*, *26*), one can assign the bands at 1215 and 1521 cm^{-1} to the F-H-F bending modes, δ, and the proton stretching

[1]Department of Chemistry, Institute for Biophysical Dynamics, and James Franck Institute, The University of Chicago, Chicago, IL 60637, USA. [2]Department of Chemistry and Cherry L. Emerson Center for Scientific Computation, Emory University, Atlanta, GA 30322, USA.
*Present address: Department of Chemistry, Yale University, New Haven, CT 06520, USA.
†Corresponding author. Email: tokmakoff@uchicago.edu

Downloaded from https://www.science.org at University of Chicago on July 03, 2023

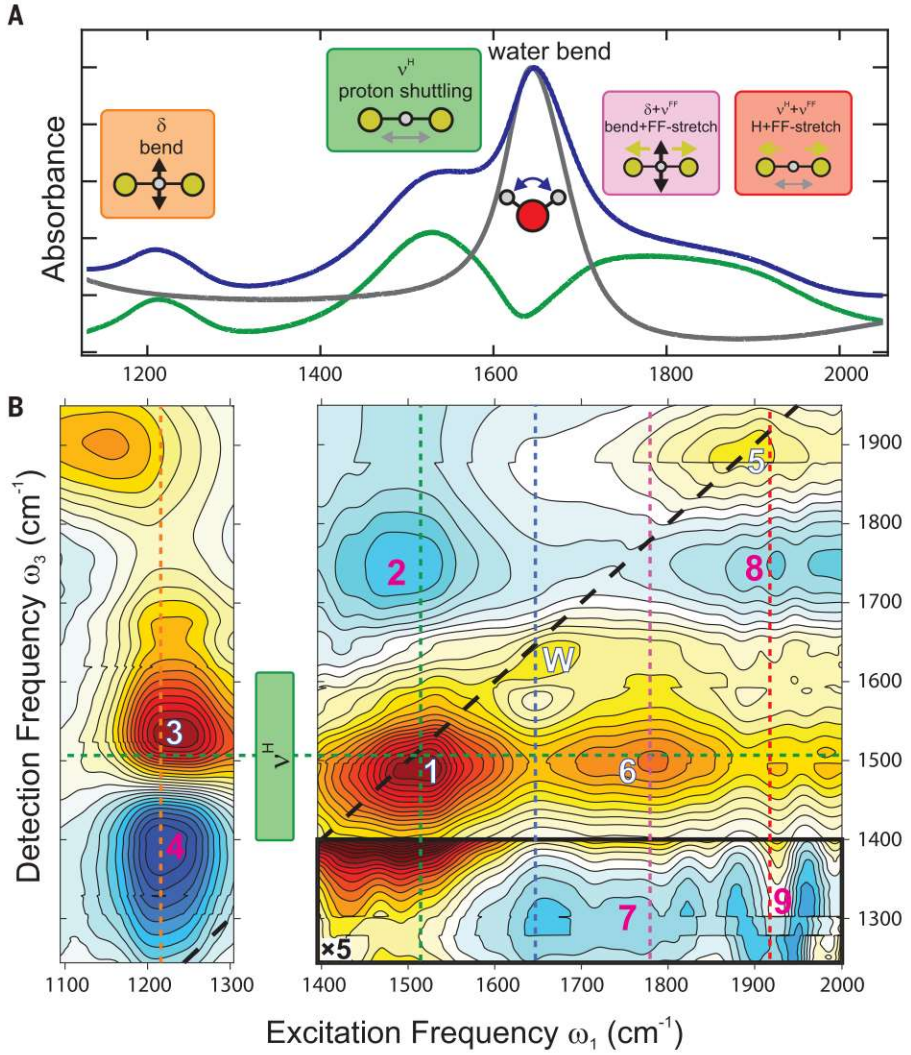

Fig. 2. IR spectroscopy of short strong H-bonds. (**A**) Linear infrared spectrum of aqueous 3.6 M KHF_2 (blue), water (gray), and their difference (green). Cartoons represent molecular motions of the respective vibrational modes. (**B**) Early-time isotropic 2D IR spectrum of 3.6 M KHF_2. Waiting times τ_2 are 150 fs (left panel) and 100 fs (right panel).

(shuttling) mode, ν^H. The H-O-H bending vibration of water appears at 1652 cm^{-1}. The broad shoulder centered at 1835 cm^{-1} shows two components in the difference spectrum. Solid-state spectrum (fig. S1B) indicates that the combination bands of F-F stretch and bending, $\delta + \nu^{FF}$, and F-F stretch and proton stretching, $\nu^H + \nu^{FF}$, are expected here. The strong anharmonicity and mode couplings have been observed in the gas-phase HF_2^- ion, where harmonic analysis at the CCSD(T) level of theory cannot even qualitatively reproduce the vibrational transitions, underestimating the proton shuttling mode by ~400 cm^{-1} (table S1). Considering the extreme anharmonicity of these short H-bonds in both gas-phase and condensed-phase systems, accurate experimental and theoretical investigations are required.

2D IR allows one to experimentally characterize the anharmonic nuclear potential by measuring the change in absorption at a detection frequency ω_3 after exciting a vibration with frequency ω_1 (Fig. 2B). The method reveals sequential transitions up the vibrational ladder, both through a decrease in absorption corresponding to the negative $|0\rangle\leftrightarrow|1\rangle$ ground-state bleach (yellow-red) and the positive $|1\rangle\rightarrow|2\rangle$ excited-state absorption (ESA) (blue). The relative placement of these features characterizes the vibrational anharmonicity. Cross-peaks in a 2D spectrum characterize the anharmonic coupling between vibrations and provide a stringent test for vibrational assignments. 2D IR has been used in this context recently to characterize the strong H-bond potential of aqueous acids (*17*, *18*).

Excitation of the proton shuttling ν^H mode at ~1400 to 1600 cm^{-1} produced an intense bleach on the diagonal (**1**) (Fig. 2B) and a $|1\rangle\rightarrow|2\rangle$ absorption peak (**2**) at higher detection frequencies (ω_1, ω_3) = (1500, 1750 cm^{-1}), indicating that γ = 1.17. This feature is a hallmark of the proton shared between two atoms in a single-well confined potential with steep walls that result in increased energy spacing between higher-lying vibrational levels. This feature is unusual because the excited-state absorption (**2**) is typically observed at lower frequencies than the bleach (**1**) and has been experimentally observed at higher frequencies only for the proton transfer mode ascribed to Zundel-like configurations of excess protons in water (*17*, *18*).

Excitation of bifluoride bending modes δ at ~1150 to 1280 cm^{-1} (Fig. 2B), followed by probing of ν^H, revealed an intense cross-peak bleach at (1240, 1510 cm^{-1}) (**3**), signifying strong coupling between the proton shuttling and bending motions. The ESA of this cross-peak at (1216, 1360 cm^{-1}) (**4**) displayed an enormous downshift of 150 cm^{-1} with respect to the bleach at 1510 cm^{-1} (γ = 0.90), an order of magnitude larger than typical molecular couplings of 10 to 15 cm^{-1} (*27*). This feature illustrates how strongly the bending of the SHB reduces the proton's confinement and confirms that bending the ion transforms the proton potential from a single well toward a strongly anharmonic double well (fig. S3B). Excitation of the broad band in the 1650 to 2000 cm^{-1} window revealed signs of two overlapping bands, which appear as peaks (**5**) and (**6**) with excitation frequencies of 1920 and 1780 cm^{-1}. These peaks appear to correspond to the expected $\nu^H + \nu^{FF}$ and $\delta + \nu^{FF}$ bands, although the intense cross-peaks to the ν^H at 1500 cm^{-1} indicate strong anharmonicities that can mix the mode character. Indeed, given the assignment of the other resonances, peaks (**8**) and (**9**) may both result from the ESA of the ν^H cross-peak. Peak (**7**) is the ESA corresponding to the ν^H cross-peak bleach (**6**).

All these observations provided direct evidence of strong interactions between all H-bond coordinates that shape the potential for the shared proton (Fig. 1B). In linear SHBs, the proton is confined and its potential is superharmonic, but H-bond bending disrupts the confinement, making it strongly positively anharmonic. Modulation of the F···F distance affects the shared proton in the SHB, causing it to experience a large-amplitude variation of its confining potential from superharmonic to strongly anharmonic.

Theoretical analysis

To quantitatively characterize the vibrational potential and spectral signatures of proton stretching in short H-bonds, we performed high-level quantum vibrational self-consistent field/virtual state configuration interaction (VSCF/VCI) calculations on $(HF_2)^-(H_2O)_6$ clusters using highly accurate many-body potential energy surface (see materials and methods)

Downloaded from https://www.science.org at University of Chicago on July 03, 2023

(*28*). To reflect the asymmetric H-bonding environment of aqueous solution, the structure of the fully solvated $(HF_2)^-(H_2O)_6$ ion with three water H-bonds to each fluorine atom was optimized, and ~1100 configurations were generated by varying F···F and F···H_2O distances. For every configuration, the proton position was optimized by holding other atoms fixed, and VSCF/VCI calculations were performed within the local monomer framework (fig. S4). The key observations are summarized in Fig. 3.

First, the transition frequencies of the key infrared resonances (Fig. 3, A to D) followed a pronounced V-shape dependence on F-F distance (d_{FF}). The calculations showed that this behavior arises from a shift between two qualitatively different types of H-bonds: SHBs for $d_{FF} \lesssim 2.4$ Å (blue, Fig. 3, A to D) and conventional H-bonds at longer separations (red). The latter showcased a textbook behavior where decreasing F-F separation strengthens the H-bond, leading to softening of the stretch potential (Fig. 3, B and C) and increased stiffness of bending modes (Fig. 3D). In this regime, the correlation of F-F distance with frequency was diffuse ($R^2 = 0.49$). Instead, the F-H distance provided a definitive correlation (Fig. 3E), corresponding to the near-linear relation between O-H distance and frequency demonstrated for a vast variety of aqueous O-H···X H-bonds (*29*).

The SHBs demonstrated the opposite effect, showing a sharp anticorrelation of F-F distance with ν^H frequency ($R^2 = 0.89$): The stronger the H-bond, the higher the proton frequency. The $\nu^H + \nu^{FF}$ frequency (Fig. 3C) followed a similar trend with the turning point at lower d_{FF}, because this mode includes F-F stretching that effectively decreases confinement compared to the ν^H mode under identical separation. These dependences upon F-F expansion are a direct consequence of the emerging barrier that approaches and exceeds the zero-point energy of the proton and localizes it in a single F-H well (Fig. 1A).

Second, the highly anharmonic character of the SHB mixes the stretching and bending motions of the H-bond, and these interactions have the maximum effect near the crossover between SHBs and conventional H-bonds (fig. S11). In this region, the ν^H potential has both steep walls and a flat bottom with the maximum value of γ reaching 1.6 (Fig. 3A), which renders it a classic example of a particle-in-a-box ($\gamma = 1.67$); the combination bands of ν^{FF} with δ or ν^H are quasi-degenerate and highly mixed, and solvation asymmetry governs the mixing. Taking the trends in the vibrational frequencies for the transitions available to experiments, we selected all configurations that mapped onto the ν^H 2D IR data (Fig. 3, F to H) and observed a close correspondence to VSCF/VCI calculations over a narrow distribution of $d_{FF} = 2.29$ to 2.31 Å in aqueous solution. This comparison indicates that peak (**6**) arose from the excitation of $\delta + \nu^{FF}$. ESA (**7**) is a unique transition to the state with all three modes excited and signifies a triple-mode coupling between all H-bond coordinates.

Third, the asymmetry of the solvent environment determines the structural asymmetry (Δ) of the HF_2^- proton position in SHBs (fig. S6) and thereby has a predictable effect on ν^H frequency (Fig. 3B and fig. S9). Asymmetric ions absorb at higher frequencies for any given d_{FF}, and a strong linear ν^H–d_{FF} anticorrelation ($R^2 = 0.97$ to 0.99) existed for any given Δ. As a result, it is the combination of changes in F-F distance and solvent asymmetry that determine ν^H in the SHB regime. Although the experimentally observed frequencies for ν^H can encompass a range of instantaneous solvent configurations, the water dynamics dictate that variations in these potentials may not be readily distinguished in these spectra. Nuclear magnetic resonance (NMR) experiments have

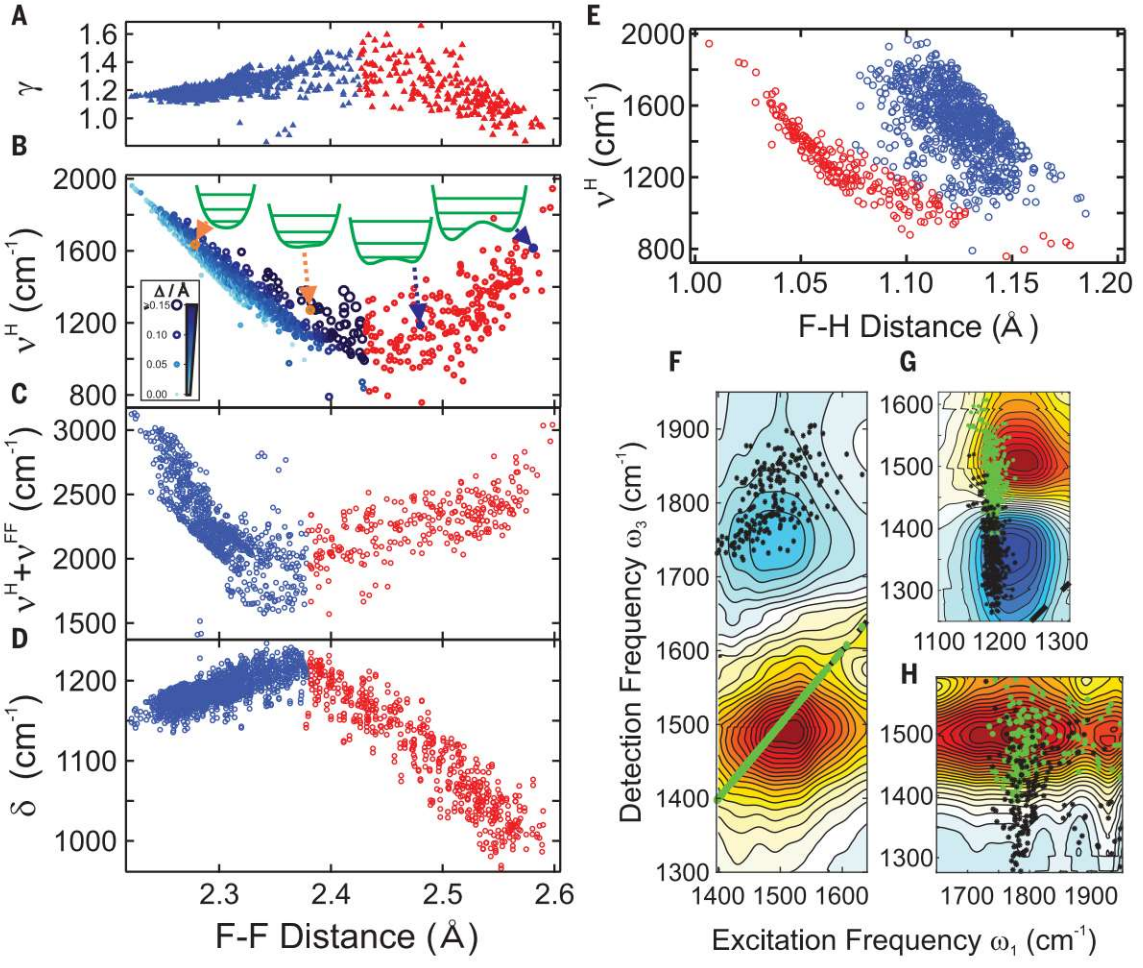

Fig. 3. Crossover from conventional H-bonds to SHBs. Influence of confinement on vibrational resonances: (**A**) γ; (**B**) ν^H (increasing proton asymmetry is mapped with color and marker size according to the legend). Proton potentials and energy levels in H-bonds at exemplary distances are shown; (**C**) $\nu^H+\nu^{FF}$; (**D**) δ modes. (**E**) Dependence of ν^H on F-H distance. SHBs are blue, conventional H-bonds are red. (**F** to **H**) Experimental ν^H bleach and ESA transitions upon excitation of (F) ν^H, (G) δ, and (H) $\delta + \nu^{FF}$ overlaid with the corresponding VSCF/VCI transition frequency distributions (green for bleach, black for ESA) for $d_{FF} = 2.29$ to 2.31 Å.

Downloaded from https://www.science.org at University of Chicago on July 03, 2023

long pointed to HF_2^- ions as the exceptional example of a symmetric centered H-bond (Δ = 0) in solution (*30*, *31*); however, these measurements average over the picosecond fluctuations in aqueous solvation environments. In principle, ultrafast 2D IR can observe a distribution of solvent environments as diagonal band elongation, but the lineshape of the ν^H diagonal bleach (**1**) is round and homogeneous at the earliest waiting time (Fig. 2B), indicating that any differences in vibrational frequency due to distance and asymmetry of configurations are essentially indistinguishable by the lineshape on the time scale of the proton's vibrational motion.

The fluctuations in solvent-induced asymmetry do shape the single-well HF_2^- proton potential, but this perturbation was below its zero-point energy (fig. S10). This observation is similar to the recent interpretation of a homogeneous lineshape for the proton stretch ESA of aqueous acids (*17*), which was attributed to the fast electric field fluctuations shaping the potential below the zero-point energy. We found that the $|1\rangle \rightarrow |2\rangle$ ESA transition was dominated by the confinement, whereas the $|0\rangle \leftrightarrow |1\rangle$ bleach signal was sensitive to both the confinement and asymmetry (fig. S9). As a result, the $(F\text{-}H\text{-}F)^-$ can be considered as a model for the Zundel limiting form of the aqueous excess proton ($H_2O\cdots H^+\cdots OH_2$) devoid of flanking water OH-stretches.

Nature of the strong H-bond

The crossover of H-bond character raises questions about when simple electrostatic descriptions of H-bonds (commonly accepted to dominate in formally ionic H-bonds, like HF_2^-) (*16*, *21*, *32*) fail and explicit treatment of their electronic structure becomes important. Figure 4A shows that as d_{FF} shrank, the magnitude of the charges decreased continuously on the proton and acceptor fluorine, while increasing on the donor fluorine for the conventional H-bonds (navy) but decreasing in the SHB regime (green). For the shortest d_{FF}, the fluorine charges approached the same value. Both electrostatic H···F attraction and F···F repulsion counterintuitively decreased upon F-F reduction in the SHBs (fig. S12), but the net electrostatic bonding was weakly dependent on d_{FF}, with a clear preference of symmetric configurations (Fig. 4B). This result is in contrast with claims that symmetric SHBs bear a high-energy penalty and are anticatalytic compared to asymmetric bonds (*20*), or that a sudden jump in bonding energy occurs when crossing from conventional to SHBs (*16*).

Electrostatics accounted for only ~52 to 62% of the SHB bonding energy, and covalent, charge-transfer, and Pauli repulsion played an increasing role at short D···A distances (fig. S13). A proper quantitative decomposition of these effects will require future work with advanced methods, like symmetry-adapted perturbation theory, although one can qualitatively understand the observed behavior with a simple molecular orbital picture. When d_{FF} decreased below 2.4 Å, F-F covalent bonding started to become a notable contributor to the SHB interactions (*33*). The hydrogen mediated this bonding, as the decreasing F-F distance enabled the overlap between the H 3s orbital and F $2p_z$ orbitals, yielding a stabilization of the resulting σ_g molecular orbital (figs. S14 and S15). This chemical bonding, consistent with other three-center four-electron bonds (*1*, *5*), is better characterized as a hydrogen-mediated donor-acceptor bond being qualitatively different from a conventional H-bond.

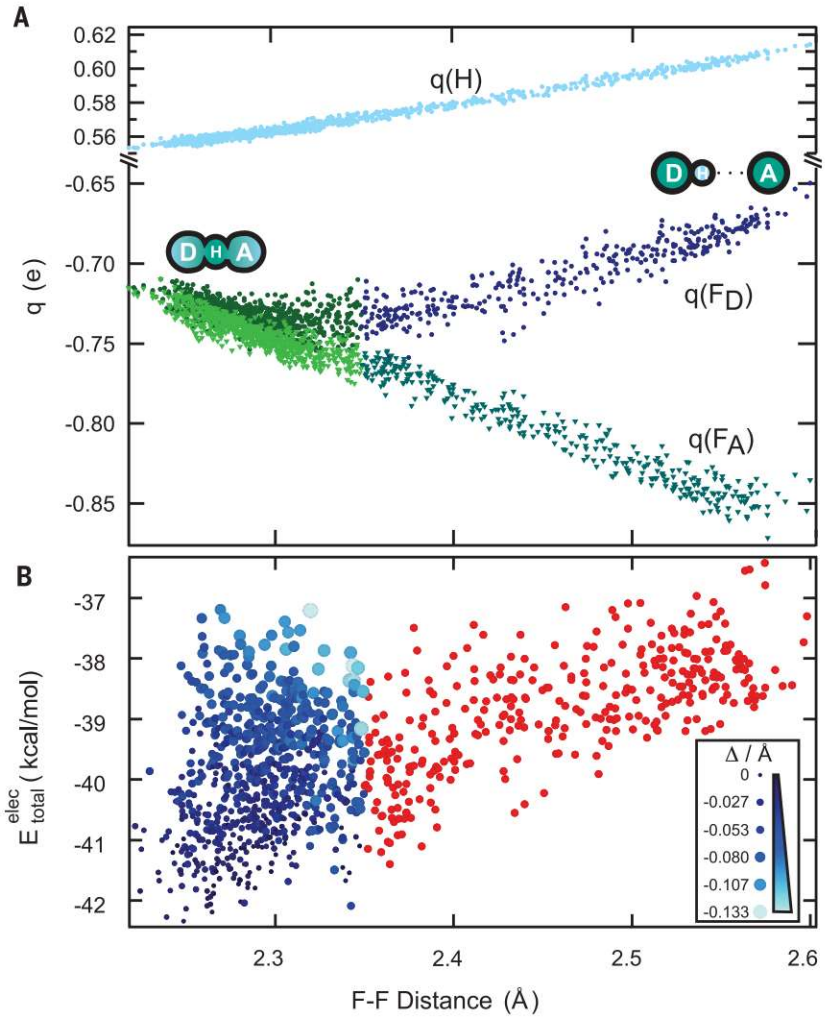

Fig. 4. Crossover from the conventional H-bonding to H-mediated chemical bonding. (**A**) Charge redistribution on constituent atoms upon donor–acceptor distance variation. (**B**) Electrostatic bonding component weakly increases with F-F distance with a preference for symmetric configurations. The proton asymmetry is encoded in the marker size and color. Conventional H-bonds are red, SHBs are blue.

Our work sheds light on the distinctive and counterintuitive properties of SHBs: delocalization of the proton in the flat-bottom confined potential that yields H-bond superharmonicity; a blueshift of the proton stretch frequency upon H-bond strengthening; and major electron density redistributions that lead to the emergence of hydrogen-mediated donor–acceptor bonding. The structural simplicity of $F\text{-}H\text{-}F^-$ system representing the bare H-bond atoms and its distinctive character as the "strongest H-bond" that one can readily describe as a chemical bond makes allowed one to identify spectroscopic trends and details of the SHB vibrational potential that will be applicable to all SHBs. Yet, $F\text{-}H\text{-}F^-$ does not suffer from the complexities that hamper the interpretation of experimental data for larger molecular systems. These results suggest that the SHB lies at the tipping point where hydrogen bonding ends and chemical bonding begins.

REFERENCES AND NOTES

1. G. C. Pimentel, *J. Chem. Phys.* **19**, 446–448 (1951).
2. A. C. Reiersolmoen *et al.*, *Chem. Sci.* **68**, 42–61 (2020).
3. P. A. Frey, S. A. Whitt, J. B. Tobin, *Science* **264**, 1927–1930 (1994).
4. W. W. Cleland, M. M. Kreevoy, *Science* **264**, 1887–1890 (1994).
5. R. H. Crabtree, *Chem. Soc. Rev.* **46**, 1720–1729 (2017).

Downloaded from https://www.science.org at University of Chicago on July 03, 2023

6. S. Yamaguchi *et al*., *Proc. Natl. Acad. Sci. U.S.A.* **106**, 440–444 (2009).
7. P. Agback, T. Agback, *Sci. Rep.* **8**, 10078 (2018).
8. P. Kumar, E. H. Serpersu, M. J. Cuneo, *Sci. Adv.* **4**, eaas8667 (2018).
9. S. Dai *et al*., *Nature* **573**, 609–613 (2019).
10. M. Elias *et al*., *Nature* **491**, 134–137 (2012).
11. S. Zhou, L. Wang, *Chem. Sci.* **10**, 7734–7745 (2019).
12. K. Mackeprang, Z.-H. Xu, Z. Maroun, M. Meuwly, H. G. Kjaergaard, *Phys. Chem. Chem. Phys.* **18**, 24654–24662 (2016).
13. Q. Yu *et al*., *J. Phys. Chem. A* **119**, 11623–11631 (2015).
14. A. Migliore, N. F. Polizzi, M. J. Therien, D. N. Beratan, *Chem. Rev.* **114**, 3381–3465 (2014).
15. G. A. Parada *et al*., *Science* **364**, 471–475 (2019).
16. F. Hibbert, J. Emsley, "Hydrogen Bonding and Chemical Reactivity" in *Advances in Physical Organic Chemistry*, D. Bethell. Ed. (Elsevier, 1990), vol. 26, pp. 255–379.
17. F. Dahms, B. P. Fingerhut, E. T. J. Nibbering, E. Pines, T. Elsaesser, *Science* **357**, 491–495 (2017).
18. J. A. Fournier, W. B. Carpenter, N. H. C. Lewis, A. Tokmakoff, *Nat. Chem.* **10**, 932–937 (2018).
19. L. M. Oltrogge, S. G. Boxer, *ACS Cent. Sci.* **1**, 148–156 (2015).
20. A. Warshel, A. Papazyan, P. A. Kollman, *Science* **269**, 102–106 (1995).
21. C. L. Perrin, *Acc. Chem. Res.* **43**, 1550–1557 (2010).
22. B. L. Van Hoozen Jr., P. B. Petersen, *J. Chem. Phys.* **148**, 134309 (2018).
23. K. Kawaguchi, E. Hirota, *J. Chem. Phys.* **87**, 6838–6841 (1987).
24. P. G. Wenthold, R. R. Squires, *J. Phys. Chem.* **99**, 2002–2005 (1995).
25. R. Newman, R. M. Badger, *J. Chem. Phys.* **19**, 1207–1208 (1951).
26. G. Pérez-Hernández, J. González-Vázquez, L. González, *J. Phys. Chem. A* **116**, 11361–11369 (2012).
27. P. Hamm, M. T. Zanni, *Concepts and Methods of 2D Infrared Spectroscopy* (Cambridge Univ. Press, New York, 2011).
28. J. M. Bowman, S. Carter, X. Huang, *Int. Rev. Phys. Chem.* **22**, 533–549 (2003).
29. M. A. Boyer *et al*., *J. Phys. Chem. Lett.* **10**, 918–924 (2019).
30. C. L. Perrin, Y. Wu, *J. Am. Chem. Soc.* **141**, 4103–4107 (2019).
31. P. Schah-Mohammedi *et al*., *J. Am. Chem. Soc.* **122**, 12878–12879 (2000).
32. M. Meot-Ner (Mautner), *Chem. Rev.* **112**, PR22–PR103 (2012).
33. L. Bytautas, T. Nagata, M. S. Gordon, K. Ruedenberg, *J. Chem. Phys.* **127**, 164317 (2007).
34. B. Dereka, Q. Yu, N. H. C. Lewis, W. B. Carpenter, J. M. Bowman, A. Tokmakoff, Crossover from hydrogen to chemical bonding, Zenodo (2020). https://doi.org/10.5281/zenodo.4060474.

ACKNOWLEDGMENTS

Funding: This work was supported by the U.S. Department of Energy grant DE-SC0014305 (B.D., N.H.C.L., W.B.C., A.T.) and the National Science Foundation grant CHE-1463552 (Q.Y., J.M.B.). Q.Y. and J.M.B. thank the Army Research Office (DURIP grant no. W911NF-14-1-0471) for funding a computer cluster where most of the calculations were performed. B.D. acknowledges the support from the Swiss National Science Foundation through Postdoc. Mobility fellowship grant P400P2_180765. **Author contributions:** B.D. and A.T. conceived the idea and designed the research. B.D. performed the experiments and analyzed the experimental data. Q.Y. developed theoretical approaches and performed calculations. B.D. and Q.Y. analyzed the theoretical results. B.D., Q.Y., N.H.C.L., W.B.C., J.M.B., and A.T. discussed and interpreted the experimental and theoretical results. J.M.B. supervised theoretical work. A.T. supervised and guided the overall research. B.D. and A.T. wrote the paper with input from all authors. **Competing interests:** None declared. **Data and materials availability:** All other data needed to evaluate the conclusions in the paper are present in the paper or the supplementary materials. All the data have been uploaded to Zenodo (*34*).

SUPPLEMENTARY MATERIALS

science.sciencemag.org/content/371/6525/160/suppl/DC1
Materials and Methods
Supplementary Text
Figs. S1 to S22
Tables S1 to S3
References (*35*–*56*)

5 August 2020; accepted 20 October 2020
10.1126/science.abe1951

Downloaded from https://www.science.org at University of Chicago on July 03, 2023

Science
AAAS

Crossover from hydrogen to chemical bonding

Bogdan Dereka, Qi Yu, Nicholas H. C. Lewis, William B. Carpenter, Joel M. Bowman, and Andrei Tokmakoff

Science, **371** (6525), .
DOI: 10.1126/science.abe1951

The nature of short hydrogen bonds

Hydrogen bonding (H-bonding) unquestionably plays an important role in chemical and biological systems and is responsible for some of their unusual properties. Strong, short H-bonds constitute a separate class that, owing to their elusive characterization, has remained a point of contention over the past several decades. Using femtosecond two-dimensional infrared spectroscopy in conjunction with quantum chemical calculations, Dereka *et al.* demonstrate a powerful way to investigate the nature of short H-bonding (see the Perspective by Bonn and Hunger). Their quantitative characterization of multiple coupled motions in the model system of bifluoride anion [F-H-F]- in aqueous solution reveals several distinctive features of a crossover from conventional to short, strong H-bonding.

Science, this issue p. 160 see also p. 123

View the article online
https://www.science.org/doi/10.1126/science.abe1951
Permissions
https://www.science.org/help/reprints-and-permissions

Downloaded from https://www.science.org at University of Chicago on July 03, 2023

Use of this article is subject to the Terms of service

Science (ISSN 1095-9203) is published by the American Association for the Advancement of Science. 1200 New York Avenue NW, Washington, DC 20005. The title *Science* is a registered trademark of AAAS.
Copyright © 2021, American Association for the Advancement of Science